his co-workers and brought into their present state by M.-H. Whangbo, T. Hughbanks, S. Wijeyesekera, M. Kertesz, C. N. Wilker, and C. Zheng. S.L. thanks Dr. G. Miller for providing us with copies of the programs and a reviewer, Dr. W. Tremel, and Prof. T. Hughbanks for their helpful comments and discussions. This work was supported by the Fonds der Chemischen Industrie.

Appendix

The extended Hückel method[16] was used in all calculations. The atomic parameters of our study are listed in Table VI. The Coulomb parameters of Er are of some interest. Values for rare-earth-metal d orbitals in previous extended Hückel studies[3c,17] range from −6.1 to −8.2 eV. The latter value would place the Er d orbitals at the same level as the C_2 π^* orbitals. In certain self-consistent studies it has been found the C_2 π^* level is filled while the rare-earth-metal levels are empty.[3d] Finally, when one compares the C_2 bond lengths of La_2C_3 and LaC_2 one finds that the C_2 bond length does not change more than 6 pm.[3e,18,19] In view of the above we place the rare-earth-metal d H_{ii} at −7 eV. We have verified that slightly lower values do not alter the overall picture presented in the current work.

Registry No. $Er_8Rh_5C_{12}$, 119147-24-9.

(16) Hoffmann, R. *J. Chem. Phys.* **1963**, *39*, 1397. (b) Whangbo, M. H.; Hoffmann, R. *J. Am. Chem. Soc.* **1978**, *100*, 6093. (c) Ammeter, J. H.; Bürgi, J.-B.; Thibeault, J. C.; Hoffmann, R. *J. Am. Chem. Soc.* **1978**, *100*, 3686.

(17) (a) Ortiz, J. V.; Hoffmann, R. *Inorg. Chem.* **1985**, *24*, 2095. A recent study on actinoide complexes is: (b) Tatsumi, K.; Nakamura, A.; Hofmann, P.; Hoffmann, R.; Moloy, K. G.; Marks, T. J. *J. Am. Chem. Soc.* **1986**, *108*, 4467.

(18) Simon, A. *J. Solid State Chem.* **1985**, *57*, 2.

(19) Atoji, M. *J. Chem. Phys.* **1961**, *35*, 1950. Atoji, M. *J. Chem. Phys.* **1961**, *35*, 1960.

(20) Burdett, J. K. *Prog. Solid State Chem.* **1985**, *15*, 173.

Contribution from the Anorganische Chemisch Laboratorium and Laboratorium voor Kristallografie, Universiteit van Amsterdam, J. H. van't Hoff Instituut, Nieuwe Achtergracht 166, 1018 WV Amsterdam, The Netherlands, and Afdeling Theoretische Chemie, Vrije Universiteit, De Boelelaan 1083, 1081 HV Amsterdam, The Netherlands

Structural, Spectroscopic, and Theoretical Studies of Novel d^6 *fac*-$Re(CO)_3LBr$ (L = Dithiooxamide) Complexes

Peter C. Servaas,[†] Derk J. Stufkens,*[,‡] Ad Oskam,[‡] Pieter Vernooijs,[§] Evert Jan Baerends,[§] Dirk J. A. De Ridder,[∥] and Caspar H. Stam[∥]

Received November 11, 1988

This article describes the syntheses and X-ray structures of three novel complexes $Re(CO)_3(DTO)Br$ (DTO = dithiooxamide), which differ in the dihedral angle θ between the thioamide groups of their DTO ligands. The structural data have been used for LCAO-Xα MO calculations on the model complex $Re(CO)_3(H_2\text{-DTO})Br$. Major differences in the structures and electronic absorption spectra are interpreted with the use of MO diagrams, orbital contour plots, calculated electronic interactions, and steric properties of the complexes. The X-ray and theoretical data show that no bonding interaction exists between the π orbitals of the thioamide groups at any dihedral angle. The thioamide π^* orbitals on the other hand interact at not too large dihedral angles, and this interaction causes the appearance of two intense electronic transitions. The predominantly Re(5d) → DTO(π^*) character of these transitions deduced from the theoretical data is confirmed by the resonance Raman spectra. The results of the MO calculations together with the X-ray structure determination of $Re(CO)_3(Cycl\text{-DTO})Br$ show that π-back-bonding from the $Re(CO)_3Br$ moiety to the lowest π^* orbital of the DTO ligand mainly occurs via an orbital with substantial (69%) Br 4p character.

Introduction

Most studies of transition-metal complexes having a lowest metal to ligand charge-transfer (MLCT) state have dealt with compounds containing members of the α-diimine family such as 2,2′-bipyridine and 1,10-phenanthroline. Our contribution in this field consisted of several studies on a series of mononuclear and dinuclear transition-metal carbonyl complexes containing these ligands.[1-6] Special attention was paid to the characterization of the metal to α-diimine charge-transfer transitions by means of resonance Raman spectra in relation to the photochemistry of these complexes.[7-10]

In all complexes studied the low-energy MLCT transitions were directed to the lowest π^* orbital of the α-diimine. Figure 1A shows the structure of *N*,*N*′-R_2-1,4-diaza-1,3-butadiene (R-DAB), which is the most simple representative of these α-diimines.

Another class of ligands also possessing a low-lying π^* orbital are the N,N′-R_2-substituted dithiooxamides (abbreviated as R_2-DTO), the general structure of which is shown in Figure 1B.

Structure determinations of several of these R_2-DTO ligands (R = Et, iPr, H)[11-14] have confirmed the planar geometry of these ligands. From the C–N and C–S bond lengths in these structures it was concluded that the R_2-DTO ligands consisted of two coupled thioamide functions. However, the relatively long central C–C

* To whom correspondence should be addressed.
† Present address: Fasson Nederland, Specialty Division, P.O. Box 28, 2300 AA Leiden, The Netherlands.
‡ Anorganisch Chemisch Laboratorium, Universiteit van Amsterdam.
§ Afdeling Theoretische Chemie, Vrije Universiteit.
∥ Laboratorium voor Kristallografie, Universiteit van Amsterdam.

(1) Balk, R. W.; Stufkens, D. J.; Oskam, A. *Inorg. Chim. Acta* **1978**, *28*, 133.
(2) Kokkes, M. W.; Stufkens, D. J.; Oskam, A. *J. Chem. Soc., Dalton Trans.* **1983**, 439.
(3) Servaas, P. C.; van Dijk, H. K.; Snoeck, Th. L.; Stufkens, D. J.; Oskam, A. *Inorg. Chem.* **1985**, *24*, 4494.
(4) Andrêa, R. R.; Luyten, H.; Vuurman, M. A.; Stufkens, D. J.; Oskam, A. *Appl. Spectrosc.* **1986**, *40*, 1184.
(5) Stufkens, D. J. Steric and Electronic Effects on the Photochemical Reactions of Metal-Metal bonded Carbonyls. In *Stereochemistry of Organometallic and Inorganic Compounds*; Bernal, I., Ed.; Elsevier: Amsterdam, 1989; Vol. 3.
(6) van Dijk, H. K.; Stufkens, D. J.; Oskam, A. *J. Am. Chem. Soc.* **1989**, *111*, 541.
(7) Balk, R. W.; Snoeck, Th. L.; Stufkens, D. J.; Oskam, A. *Inorg. Chem.* **1980**, *19*, 3015.
(8) Balk, R. W.; Stufkens, D. J.; Oskam, A. *J. Chem. Soc., Dalton Trans.* **1981**, 1124.
(9) van Dijk, H. K.; Servaas, P. C.; Stufkens, D. J.; Oskam, A. *Inorg. Chim. Acta* **1985**, *104*, 179.
(10) Servaas, P. C.; Stufkens, D. J.; Oskam, A. *Inorg. Chem.* **1989**, *28*, 1780.
(11) Drew, M. G. B.; Kisenyi, J. M.; Willey, G. R. *J. Chem. Soc., Dalton Trans.* **1982**, 1729.
(12) Drew, M. G. B.; Kisenyi, J. M.; Willey, G. R.; Wandiga, S. O. *J. Chem. Soc., Dalton Trans.* **1984**, 1717.
(13) Wheatley, P. J. *J. Chem. Soc.* **1965**, 396.
(14) Mo, F.; Thorkildsen, G. *Acta Crystallogr., Sect. A* **1984**, *A40*, C160.

0020-1669/89/1328-4104$01.50/0

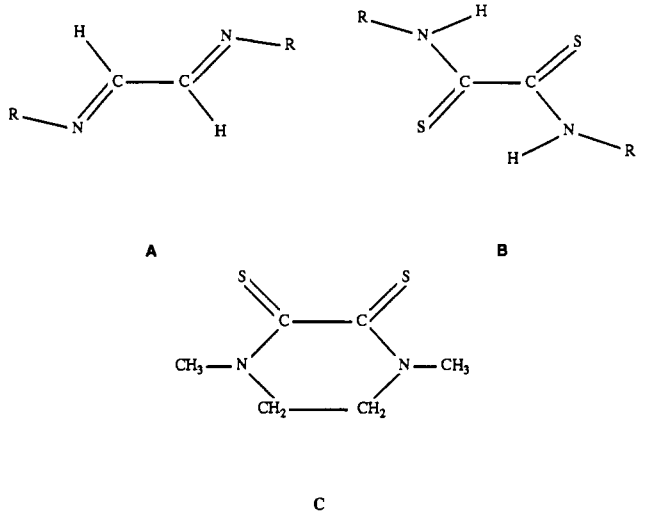

Figure 1. Structure of *E-s-trans-E*-R-DAB (A), *E-s-trans-E*-R_2-DTO (B), and Cycl-DTO (C).

bond lengths of 1.50–1.54 Å revealed that in the electronic ground state no net delocalization of π electrons occurs between the two thioamide moieties. Recently, theoretical data on the electronic structure and bonding of H_2-DTO have been reported by Green et al.[15] From their results it can be concluded that the four occupied π orbitals of *s-trans*-H_2-DTO do not give rise to π bonding along the central C–C bond.

A large number of publications have appeared on transition-metal dithiooxamide complexes,[15-21] but in only a few of them the DTO ligand acts as a neutral bidentate donor ligand and without hydrogen bonds to other, e.g. halide, ligands. From the electronic absorption and infrared spectra of a series of Mo(CO)$_{4-n}$(PR$_3$)$_n$L complexes (n = 0, 1, 2; L = dithiooxamide) it was concluded that in most of these complexes the DTO ligand acts as a relatively strong donor ligand, albeit with a low-lying π^*-acceptor level.[20] Furthermore, it was recently demonstrated from the crystal structures of [Cu(Bzl$_2$-DTO)$_2$][ClO$_4$]$_2$ (Bzl = benzyl) and Zn(Me$_2$-DTO)Cl$_2$ that these ligands do not possess a planar geometry when they are S,S′-coordinated to a metal center as *s-cis*-R_2-DTO.[21] In fact, in these complexes such a planarity is prohibited by the steric hindrance between the two amide protons, requiring a dihedral angle of at least 36° between the thioamide moieties.

In order to elucidate the electronic and structural properties of neutral DTO ligands in transition-metal (carbonyl) complexes, we studied several *fac*-Re(CO)$_3$LBr (L = dithiooxamide) complexes in more detail. As a representative of the R_2-DTO class of ligands (Figure 1B), we have used Bzl$_2$-DTO. Furthermore, the cyclic DTO ligand *N,N′*-dimethylpiperazine-2,3-dithione (=Cycl-DTO, **1**; see Figure 1C) and its complex Re(CO)$_3$(Cycl-DTO)Br (**2**) were synthesized, for which no steric hindrance between the thioamide groups is expected. It will be shown that with this cyclic ligand indeed an almost planar geometry is achieved upon coordination to the metal center. On the other hand, by using Et$_4$-DTO as a ligand with four equal R groups, we could prepare a complex having a strongly distorted DTO geometry.

Table I. Analytical Data for Re(CO)$_3$LBr (L = Dithiooxamide) Complexes

complex		anal.[a] found (calcd)	IR: ν(CO)/cm^{-1} [b]	^{1}H NMR: δ/ppm[c]
2	C	21.76 (20.61)	2020, 1929, 1898	4.28 (s, 4 H), 3.74 (s, 6 H)
	H	2.14 (1.92)		
	N	5.26 (5.34)		
3	C	27.51 (26.81)	2021, 1919, 1895	4.97 (m, 1 H), 4.32 (m, 1 H), 3.94–3.42 (m, 6 H), 1.60–1.21 (m, 12 H)
	H	3.49 (3.46)		
	N	4.79 (4.81)		
	O	8.35 (8.24)		
	Br	13.70 (13.72)		
4	C	34.72 (35.08)	2021, 1929, 1899	11.0 (s, 1 H), 7.40 (m, 10 H), 5.00 (d, 4 H)
	H	2.46 (2.48)		
	N	4.21 (4.31)		

[a] In percent. [b] Values obtained in THF solutions. [c] Values (relative to TMS) obtained in acetone-d_6.

In this article we report the syntheses, structures, and spectroscopic (UV/visible, IR, ^{1}H NMR, resonance Raman) properties of these complexes as well as the results of LCAC–Xα MO calculations. The photochemistry will be presented in a forthcoming article.[22]

Experimental Section

Preparations. The ligands Cycl-DTO (**1**) (Figure 1C), Bzl$_2$-DTO, and Et$_4$-DTO were synthesized according to literature procedures.[23,24] The syntheses of the Re(CO)$_3$(DTO)X (X = Cl, Br) complexes are described hereafter, and their analytical data are summarized in Table I. The complexes are all moderately air stable, but their solutions had to be treated under a nitrogen atmosphere in order to prevent a slow decomposition.

Re(CO)$_3$(Cycl-DTO)Br (2). Re(CO)$_5$Br (2.46 mmol) and Cycl-DTO (**1**) (2.87 mmol) were refluxed under a N_2 atmosphere in 50 mL of toluene for 3 h. After filtration at room temperature the residue was purified by column chromatography (silica; toluene). The complex was dissolved in THF, and the THF solution was injected on top of the silica column, elution with toluene/THF (1:1) yielding the unreacted starting compounds. After subsequent elution with acetone a deep red fraction was obtained. Evaporation in vacuo yielded 91% of Re(CO)$_3$(Cycl-DTO)Br (1.17 g), which was identified by elemental analysis and IR and ^{1}H NMR spectroscopy (Table I) and by an X-ray structure determination (see below).

Re(CO)$_3$(Et$_4$-DTO)Br (3). Re(CO)$_5$Br (1.35 mmol) and Et$_4$-DTO (1.38 mmol) were refluxed under a N_2 atmosphere in 40 mL of toluene for 4 h. After filtration at room temperature the residue was washed successively with toluene and *n*-pentane. Evaporation in vacuo yielded 91% of Re(CO)$_3$(Et$_4$-DTO)Br (0.72 g), which was identified by elemental analysis and IR and ^{1}H NMR spectroscopy (Table I) and by an X-ray structure determination (see below).

Re(CO)$_3$(Bzl$_2$-DTO)Br (4). Re(CO)$_5$Br (1.52 mmol) and Bzl$_2$-DTO (1.90 mmol) were refluxed for 2 h under a N_2 atmosphere in 40 mL of toluene. After filtration at room temperature the residue was washed several times with 10-mL portions of *n*-hexane. Evaporation in vacuo yielded 83% of Re(CO)$_3$(Bzl$_2$-DTO)Br (0.82 g), which was identified by elemental analysis and IR and ^{1}H NMR spectroscopy (Table I).

Re(CO)$_3$(Cycl-DTO)Cl (5) (in Situ). Re(CO)$_3$(Cycl-DTO)Br (24 mg) and silver trifluoromethanesulfonate (AgOTF; 12 mg) were stirred for 1 h at room temperature in 15 mL of acetone. The IR spectrum of the solution then indicated a complete conversion of the parent complex (ν(CO): 2020, 1926, and 1898 cm^{-1} in acetone) into Re(CO)$_3$(Cycl-DTO)$^+$(OTF)$^-$(ν(CO): 2031, 1931, and 1918 cm^{-1}). After filtration 7.55 mg of tetraethylammonium chloride was added to the filtrate and the solution was stirred for another 1 h. The IR spectrum of the solution then indicated a complete conversion into Re(CO)$_3$(Cycl-DTO)Cl (ν(CO): 2019, 1924, and 1896 cm^{-1}).

(15) Green, M. R.; Jubran, N.; Bursten, B. E.; Busch, D. H. *Inorg. Chem.* **1987**, *26*, 2326.
(16) Wandiga, S. O.; Jenkins, L. S.; Willey, G. R. *J. Inorg. Nucl. Chem.* **1979**, *41*, 941.
(17) Hofmans, H.; Desseyn, H. O.; Herman, M. A. *Spectrochim. Acta, Part A* **1982**, *38A*, 1307.
(18) Drew, M. G. B.; Kisenyi, J. M.; Willey, G. R. *J. Chem. Soc., Dalton Trans.* **1984**, 1723.
(19) Ferrari, M. B.; Fava, G. G.; Pelizzi, C.; Tarasconi, P. *Inorg. Chim. Acta* **1985**, *98*, L49.
(20) tom Dieck, H.; Form, M. *Z. Anorg. Allg. Chem.* **1984**, *515*, 19.
(21) Antolini, L.; Fabretti, A. C.; Franchini, G.; Menabue, L.; Pellacani, G. C.; Desseyn, H. O.; Dommisse, R.; Hofmans, H. C. *J. Chem. Soc., Dalton Trans.* **1987**, 1921.
(22) Servaas, P. C.; Stufkens, D. J.; Oskam, A. To be submitted for publication.
(23) Isaksson, R.; Liljefors, T.; Sandström, J. *J. Chem. Res., Miniprint* **1981**, 664.
(24) Hurd, R. N.; De La Mater, G.; McElheny, G. C.; Turner, R. J.; Wallingford, V. H. *J. Org. Chem.* **1961**, *26*, 3980.

Table II. Crystallographic Data and Refinement Details

	1	2	3
	(a) Crystal Data		
formula	$C_6H_{10}N_2S_2$	$C_9H_{10}BrN_2O_3ReS_2$	$C_{13}H_{20}BrN_2O_3ReS_2$
M_r	174.29	524.43	582.55
cryst class	monoclinic	monoclinic	monoclinic
space group	*Aa*	$P2_1/n$	$P2_1/n$
a/Å	10.653 (1)	16.998 (3)	18.561 (7)
b/Å	7.2937 (6)	9.166 (1)	14.535 (5)
c/Å	10.640 (1)	9.637 (4)	7.006 (2)
β/deg	95.26 (1)	105.47 (2)	92.56 (6)
V/Å^3	823.2 (2)	1447.1 (7)	1888 (2)
F(000)	368	976	1112
D_x/g cm^{-3}	1.42	2.41	2.05
Z	4	4	4
cryst size/mm	0.25 × 0.20 × 0.13	0.30 × 0.20 × 0.08	0.35 × 0.13 × 0.03
	(b) Data Collection		
radiation	Cu Kα	Mo Kα	Mo Kα
θ range/deg	2.5–70	1.1–30	1.1–25
data set	h, −12→12; k, 0→8; l, 0→12	h, −23→23; k, 0→12; l, 0→13	h, −22→22; k, 0→17; l, 0→8
no. of collcd reflcns	770	4177	3290
no. of obsd reflcns	714 ($I > 2.5\sigma(I)$)	2598 ($I > 2.5\sigma(I)$)	2160 ($I > 2.5\sigma(I)$)
abs cor	not applied	applied[a]	applied[a]
	(c) Refinement (Structure Determination)		
non-H atoms	anisotropic	anisotropic	anisotropic
H atoms	isotropic	isotropic	isotropic
w[b]	$1/[1.92 + F_o + 0.006F_o^2]$	$1/[5.56 + F_o + 0.029F_o^2]$	$1/[4.94 + F_o + 0.047F_o^2]$
R	0.035	0.042	0.073
R_w	0.040	0.088	0.136

[a] An empirical absorption correction (DIFABS) has been applied (see ref 32). [b] F_o = observed structure factor value.

Spectra. Standard inert-gas techniques were used to prepare the spectroscopic samples. The solvents, which were all of a spectroscopic grade, were distilled several times and carefully oxygenated before use. The UV/visible spectra were measured on a Perkin-Elmer Lambda 5 spectrophotometer, IR spectra on a Nicolet 7199B FT-IR interferometer with a liquid-cooled Hg, Cd, Te detector (32 scans, resolution 0.5 cm^{-1}), and ^{1}H NMR spectra on a Bruker AC 100 spectrometer. The resonance Raman spectra were recorded on a Jobin Yvon HG2S Ramanor spectrophotometer by using an SP Model Ar^+ ion laser as the excitation source. An Anaspec 300-S with a band pass of 0.4 nm was used a premonochromator. The spectra were recorded with a spinning cell.

MO Calculations. Molecular orbital calculations were performed with the Hartree–Fock–Slater (LCAO–Xα) method,[25,26] which, contrary to the Hartree–Fock method, uses Slater's $\rho^{1/3}$ or Xα exchange potential instead of the full HF exchange operator. In this method the molecular orbitals were expanded as a linear combination of Slater type orbitals (STO). The applicability of this HFS method in organometallic chemistry has been demonstrated in a number of reports.[27-30] An uncontracted triple-ζ STO basis set was employed for Re 5d (exponents 1.4, 2.5, and 4.4) and standard double-ζ sets for Re 6s, C, N, and O 2s and 2p, S 3s and 3p, H 1s, and Br 4s and 4p. D-type polarization functions have been added to the C, N, and S atoms of DTO (exponents ζ^{C}_{3d} = 2.0, ζ^{N}_{3d} = 2.0, ζ^{S}_{3d} = 2.2) and to Br (ζ^{Br}_{4d} = 2.0). P-type polarization functions have been added to Re (ζ^{Re}_{6p} = 1.73) and H (ζ^{H}_{2p} = 1.0). The lower shells were considered as a core and kept frozen according to the procedure of ref 25. Furthermore, we used an auxiliary basis of density-fitting functions and special numerical integration techniques to evaluate the Fock matrix. The computational scheme affords an essentially ab initio calculation of the wave function, the quality of which thus depends on the HFS model and the size of the above-mentioned basis set.

In order to keep the calculations tractable, H_2-DTO was used as the DTO ligand. For $Re(CO)_3(H_2\text{-DTO})Br$ the fragments $Re(CO)_3Br$ and *cis*-H_2-DTO have been used. In the calculations on the "ligands" *trans*-H_2-DTO (θ = 180°), $\perp$-H_2-DTO (θ = 90°), and *cis*-H_2-DTO (θ = 0°), for similar reasons two $^{\bullet}CSNH_2$ fragments were used. Although this treatment implies that the results will have qualitative rather than quantitative significance, good agreement was obtained for *trans*-H_2-DTO between the calculated and experimental values for ionization potentials (IP's) and excitation energies.

In the calculations on free H_2-DTO, bond distances and angles have been used from the X-ray structural data of H_2-DTO.[13,14] On a similar basis results from the X-ray structural data of **2** were applied for the $Re(CO)_3(H_2\text{-DTO})Br$ complex, for which a C_s symmetry was adopted with the H_2-DTO ligand fully in-plane with the equatorial CO groups.

Crystal Structure Determination of 1–3. All diffraction data were measured on an Enraf-Nonius CAD4 diffractometer using graphite-monochromated Cu Kα (λ = 1.5418 Å, structure **1**) or Mo Kα (λ = 0.710 69 Å, structures **2** and **3**) radiation. The further experimental details of the structure determinations of these molecules are given in Table II.

The structures were solved by means of the heavy-atom method. For all structures a block-diagonal least-squares refinement on F was carried out.

Negative temperature factors in **3** for the CO group trans to the Br atom and a difference-Fourier synthesis with a value of ρ that varied between −3.2 and 5.2 e Å^{-3} suggested disorder along the CO–Re–Br axis. Inspection of a difference-Fourier map in this region indicated that the disorder was caused by a superposition of two isomers, differing from each other by opposite positions of the axial CO and Br ligands but showing equal structural features of the rhenium–dithiooxamide moieties. CO and Br have roughly equal spatial requirements in relation to the surrounding structure, the centers of the electron distributions of CO and Br being at about the same distance from Re. Isotropic refinement with a coupled population parameter for Br and $(CO)_3$, with the temperature factor for these atoms being fixed at U = 0.038 converged to R = 0.101.

An empirical absorption correction was applied on structures **2** and **3**.[31] For all structures a weighing scheme was used and the anomalous dispersion of S was taken into account for **1** and those of Re and Br were taken into account for **2** and **3**. The calculations were carried out with XRAY76,[32] the scattering factors and the dispersion correction were taken from ref 33. The final positional parameters and the equivalent isotropic

(25) Baerends, E. J.; Ellis, D. E.; Ros, P. *Chem. Phys.* **1973**, *2*, 41.
(26) Baerends, E. J.; Ros, P. *Int. J. Quantum Chem.* **1978**, *S12*, 169.
(27) Baerends, E. J.; Rozendaal, A. Analysis of σ-bonding, π-(back)bonding and the synergic effect in $Cr(CO)_6$. Comparison of Hartree-Fock and Xα results for metal-CO bonding. In *Quantum Chemistry: The Challenge of Transition Metals and Coordination Chemistry*; Veillard, A., Ed.; Reidel: Dordrecht, The Netherlands, 1986; p 159.
(28) Olthoff, J. K.; Moore, J. H.; Tossell, J. A.; Giordon, J. C.; Baerends, E. J. *J. Chem. Phys.* **1987**, *87*, 7001.
(29) Boerrigter, P. M.; Baerends, E. J.; Snijders, J. G. *Chem. Phys.* **1988**, *122*, 357.
(30) Ziegler, T.; Tschinke, V.; Versluis, L.; Baerends, E. J. *Polyhedron* **1988**, *7*, 1625.
(31) Walker, W.; Stuart, D. *Acta Crystallogr., Sect. A: Found. Crystallogr.* **1983**, *A39*, 158.
(32) Stewart, J. M. "The X-Ray 76 System"; Technical Report Tr44, 1976; Computer Science Center, University of Maryland, College Park, MD.
(33) Cromer, D. T.; Mann, J. B. *International Tables for X-Ray Crystallography*; Kynoch Press: Birmingham, England, 1974; Vol. IV, p 55.

Table III. Final Positional and Equivalent Isotropic Thermal Parameters of the Non-Hydrogen Atoms of **1–3** with Esd's in Parentheses

atom	*x*	*y*	*z*	U_{eq}/Å^2
		1		
S(1)	0.1116 (1)	0.1805 (2)	0.0581 (1)	0.0466 (7)
S(2)	0.3885 (1)	0.1801 (2)	−0.0602 (1)	0.0460 (7)
C(1)	0.1982 (4)	0.3689 (7)	0.0449 (4)	0.032 (2)
C(2)	0.3031 (4)	0.3677 (7)	−0.0444 (4)	0.032 (2)
C(3)	0.2539 (6)	0.6888 (8)	−0.0708 (7)	0.055 (4)
C(4)	0.2460 (6)	0.6951 (8)	0.0670 (7)	0.057 (4)
C(5)	0.4082 (6)	0.5373 (10)	−0.2014 (5)	0.057 (4)
C(6)	0.0918 (6)	0.5463 (10)	0.2000 (6)	0.058 (4)
N(1)	0.1829 (4)	0.5267 (6)	0.1028 (4)	0.040 (2)
N(2)	0.3212 (4)	0.5223 (6)	−0.1061 (4)	0.041 (2)
		2		
Re	0.34876 (3)	0.17353 (5)	0.20851 (5)	0.0302 (2)
Br	0.3798 (1)	0.2208 (2)	−0.0423 (2)	0.0534 (9)
S(1)	0.3948 (2)	0.4253 (4)	0.2695 (4)	0.040 (2)
S(2)	0.4958 (2)	0.1215 (4)	0.3003 (5)	0.042 (2)
C(1)	0.3248 (7)	−0.023 (2)	0.149 (2)	0.038 (7)
C(2)	0.2367 (9)	0.229 (2)	0.129 (2)	0.039 (7)
C(3)	0.3262 (9)	0.136 (1)	0.392 (1)	0.037 (6)
C(4)	0.5384 (8)	0.284 (1)	0.278 (1)	0.032 (6)
C(5)	0.4951 (7)	0.424 (1)	0.282 (1)	0.028 (5)
C(6)	0.651 (1)	0.152 (2)	0.228 (2)	0.051 (9)
C(7)	0.502 (1)	0.687 (2)	0.314 (2)	0.054 (10)
C(8)	0.6511 (10)	0.426 (2)	0.242 (2)	0.052 (9)
C(9)	0.6283 (8)	0.538 (2)	0.334 (2)	0.038 (7)
N(1)	0.6102 (6)	0.284 (1)	0.251 (1)	0.034 (5)
N(2)	0.5395 (7)	0.541 (1)	0.304 (1)	0.036 (6)
O(1)	0.3101 (8)	−0.141 (1)	0.103 (1)	0.053 (7)
O(2)	0.1712 (6)	0.261 (2)	0.081 (1)	0.058 (7)
O(3)	0.3110 (9)	0.113 (1)	0.493 (1)	0.061 (7)
		3[a]		
Re	0.11333 (5)	0.19027 (6)	0.0881 (1)	0.0329 (5)
S(1)	0.1508 (4)	0.2624 (4)	−0.2266 (9)	0.038 (3)
S(2)	0.2124 (4)	0.2879 (4)	0.2422 (9)	0.037 (3)
C(1)	0.041 (1)	0.110 (1)	−0.060 (5)	0.05 (2)
C(2)	0.085 (1)	0.133 (2)	0.318 (4)	0.05 (2)
C(4)	0.177 (2)	0.361 (1)	−0.110 (4)	0.04 (1)
C(5)	0.238 (1)	0.344 (2)	0.042 (4)	0.03 (1)
C(6)	0.163 (2)	0.518 (2)	0.020 (4)	0.05 (2)
C(7)	0.185 (2)	0.600 (2)	−0.094 (4)	0.07 (2)
C(8)	0.083 (2)	0.449 (3)	−0.260 (4)	0.09 (3)
C(9)	0.103 (2)	0.474 (2)	−0.463 (4)	0.06 (2)
C(10)	0.365 (2)	0.348 (2)	0.142 (5)	0.06 (2)
C(11)	0.389 (2)	0.257 (2)	0.139 (5)	0.07 (2)
C(12)	0.321 (2)	0.422 (2)	−0.180 (4)	0.05 (2)
C(13)	0.374 (2)	0.369 (2)	−0.286 (5)	0.07 (2)
N(1)	0.149 (1)	0.438 (1)	−0.114 (3)	0.04 (1)
N(2)	0.3023 (10)	0.371 (1)	0.007 (3)	0.03 (1)
O(1)	0.000 (1)	0.072 (2)	−0.133 (4)	0.07 (1)
O(2)	0.067 (2)	0.105 (2)	0.462 (3)	0.09 (2)
Br(a)	0.0180 (2)	0.3231 (3)	0.1277 (6)	0.038 (0)
C(3a)	0.176 (2)	0.098 (3)	0.093 (6)	0.038 (0)
O(3a)	0.235 (2)	0.080 (2)	0.062 (4)	0.038 (0)
Br(b)	0.2102 (3)	0.0603 (4)	0.0762 (8)	0.038 (0)
C(3b)	0.055 (3)	0.284 (4)	0.104 (8)	0.038 (0)
O(3b)	0.012 (2)	0.334 (3)	0.049 (6)	0.038 (0)

[a] Population parameters $a = 0.56$ and $b = 0.44$.

Table IV. Selected Bond Distances (Å) and Angles (deg) of **1** with Esd's in Parentheses

S(1)–C(1)	1.668 (4)	C(3)–C(4)	1.477 (7)
S(2)–C(2)	1.660 (4)	C(3)–N(2)	1.476 (5)
C(1)–C(2)	1.532 (5)	C(4)–N(1)	1.467 (5)
C(1)–N(1)	1.323 (5)	C(5)–N(2)	1.439 (5)
C(2)–N(2)	1.328 (5)	C(6)–N(1)	1.489 (5)
S(1)–C(1)–C(2)	119.2 (3)	C(3)–C(4)–N(1)	107.5 (4)
S(1)–C(1)–N(1)	125.8 (3)	C(1)–N(1)–C(4)	121.9 (4)
C(2)–C(1)–N(1)	115.0 (3)	C(1)–N(1)–C(6)	121.5 (4)
S(2)–C(2)–N(2)	123.0 (3)	C(4)–N(1)–C(6)	116.3 (4)
S(2)–C(2)–C(1)	120.3 (3)	C(2)–N(2)–C(3)	118.5 (4)
C(1)–C(2)–N(2)	116.7 (3)	C(2)–N(2)–C(5)	123.0 (4)
C(4)–C(3)–N(2)	110.6 (4)	C(3)–N(2)–C(5)	118.4 (4)

Table V. Selected Bond Distances (Å) and Angles (deg) of **2** with Esd's in Parentheses

Re–Br	2.643 (1)	C(3)–O(3)	1.09 (1)
Re–S(1)	2.457 (3)	C(4)–C(5)	1.48 (1)
Re–S(2)	2.465 (3)	C(4)–N(1)	1.31 (1)
Re–C(1)	1.90 (1)	C(5)–N(2)	1.30 (1)
Re–C(2)	1.92 (1)	C(6)–N(1)	1.44 (1)
Re–C(3)	1.937 (10)	C(7)–N(2)	1.50 (1)
S(2)–C(4)	1.695 (10)	C(8)–C(9)	1.47 (2)
C(1)–O(1)	1.17 (1)	C(8)–N(1)	1.49 (2)
C(2)–O(2)	1.12 (1)	C(9)–N(2)	1.46 (1)
Br–Re–S(1)	86.3 (1)	Re–C(1)–O(1)	175.4 (8)
Br–Re–S(2)	85.9 (1)	Re–C(2)–O(2)	179.2 (8)
Br–Re–C(1)	87.6 (4)	Re–C(3)–O(3)	177.6 (8)
Br–Re–C(2)	90.6 (4)	S(2)–C(4)–C(5)	121.7 (8)
Br–Re–C(3)	179.2 (3)	S(2)–C(4)–N(1)	118.4 (8)
S(1)–Re–S(2)	82.4 (1)	C(5)–C(4)–N(1)	119.9 (10)
S(1)–Re–C(2)	93.8 (4)	S(1)–C(5)–C(4)	120.4 (8)
S(1)–Re–C(3)	94.4 (4)	S(1)–C(5)–N(2)	117 (1)
S(2)–Re–C(1)	92.3 (4)	C(9)–C(8)–N(1)	112 (1)
S(2)–Re–C(2)	175.0 (3)	C(8)–C(9)–N(2)	109 (1)
S(2)–Re–C(3)	93.8 (5)	C(4)–N(1)–C(6)	123 (1)
C(1)–Re–C(2)	91.2 (6)	C(4)–N(1)–C(8)	119 (1)
C(1)–Re–C(3)	91.6 (6)	C(6)–N(1)–C(8)	118 (1)
C(2)–Re–C(3)	89.7 (7)	C(5)–N(2)–C(7)	121 (1)
Re–S(1)–C(5)	105.3 (4)	C(5)–N(2)–C(9)	122.9 (10)
Re–S(2)–C(4)	102.2 (5)	C(7)–N(2)–C(9)	116 (1)

Table VI. Selected Bond Distances (Å) and Angles (deg) of **3** with Esd's in Parentheses

Re–S(1)	2.567 (4)	C(4)–N(1)	1.23 (2)
Re–S(2)	2.526 (5)	C(5)–N(2)	1.29 (2)
Re–C(1)	2.03 (2)	C(6)–C(7)	1.50 (3)
Re–C(2)	1.91 (2)	C(6)–N(1)	1.51 (2)
Re–Br(a)	2.642 (3)[a]	C(10)–N(2)	1.50 (3)
Re–C(3a)	1.77 (3)[a]	C(12)–C(13)	1.48 (3)
Re–Br(b)	2.612 (4)[a]	C(12)–N(2)	1.56 (2)
Re–C(3b)	1.75 (4)[a]	C(10)–C(11)	1.40 (3)
S(1)–C(4)	1.71 (2)	C(8)–N(1)	1.57 (3)
S(2)–C(5)	1.71 (2)	C(8)–C(9)	1.53 (3)
C(1)–O(1)	1.05 (2)	C(3a)–O(3a)	1.16 (4)[a]
C(2)–O(2)	1.15 (3)	C(3b)–O(3b)	1.13 (5)[a]
C(4)–C(5)	1.54 (3)		
S(1)–Re–S(2)	85.2 (2)	S(1)–C(4)–C(5)	112 (1)
S(1)–Re–C(1)	89.7 (9)	S(1)–C(4)–N(1)	130 (1)
S(1)–Re–C(2)	178.2 (6)	C(5)–C(4)–N(1)	117 (2)
S(2)–Re–C(1)	173.7 (5)	S(2)–C(5)–C(4)	115 (1)
S(2)–Re–C(2)	96.1 (8)	S(2)–C(5)–N(2)	127 (1)
C(1)–Re–C(2)	89 (1)	C(4)–C(5)–N(2)	119 (2)
Br(a)–Re–C(3a)	172.6 (10)[a]	C(7)–C(6)–N(1)	109 (2)
Br(b)–Re–C(3b)	175 (1)[a]	C(9)–C(8)–N(1)	115 (2)
Re–C(3a)–O(3a)	142 (2)[a]	C(11)–C(10)–N(2)	116 (2)
Re–C(3b)–O(3b)	155 (3)[a]	C(13)–C(12)–N(2)	111 (2)
C(10)–N(2)–C(12)	116 (2)	C(4)–N(1)–C(6)	129 (2)
Re–S(1)–C(4)	90.8 (9)	C(4)–N(1)–C(8)	115 (2)
Re–S(2)–C(5)	98.1 (8)	C(6)–N(1)–C(8)	116 (2)
Re–C(1)–O(1)	175 (1)	C(5)–N(2)–C(12)	123 (2)
Re–C(2)–O(2)	175 (2)	C(5)–N(2)–C(10)	121 (2)

[a] These values are unreliable due to disorder along the Br–Re–CO_{ax} axis.

thermal parameters for the non-hydrogen atoms are given in Table III. The selected bond distances and angles of **1–3** are collected in Tables IV–VI, respectively.

Results

Molecular Structures. 1. Cycl-DTO (1). Generally, dithiooxamide molecules are built up by two thioamide moieties. The dihedral angle θ between these groups can vary depending on the substituents R at the nitrogen atoms. For *N,N'*-R_2-DTO molecules crystal structures have confirmed an s-trans conformation in these molecules ($\theta = 180°$).[11-14] On the other hand, for *N,N*-Me_2-DTO (i.e. with both methyl groups bonded to one of the nitrogen atoms) the thioamide groups are almost perpendicular ($\theta = 93.1°$), which is probably caused by steric hindrance between the methyl groups

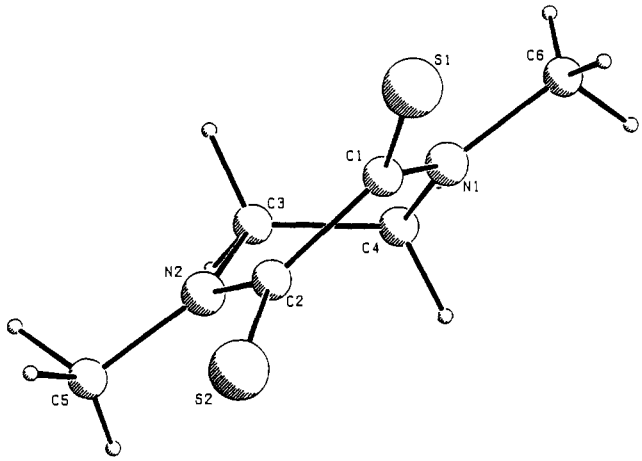

Figure 2. Crystal structure of Cycl-DTO (**1**).

and the sulfur atoms.[34] A similar configuration was also reported for the Me_4-substituted oxamide (θ = 71.4°) and Me_4-substituted thiooxamide (θ = 87.4°).[35]

For Cycl-DTO (**1**) the presence of a ring system imposes a cis conformation. Figure 2 shows the structure of **1** with a calculated dihedral angle θ of 35.4°. This value is close to that of 31° predicted by Hendriksen et al. for this molecule using molecular mechanics calculations.[36]

The mean bond lengths in the thioamide groups are C–S = 1.664 (6) Å and C–N = 1.326 (4) Å, respectively.[37] These values, like those previously reported for other DTO ligands,[11-14,35] confirm the importance of resonance configurations of the type:

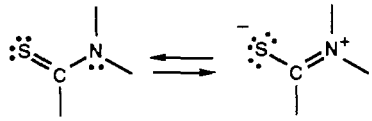

The C(1)–C(2) distance of 1.532 (5) Å between the two thioamide functions is significantly larger than the values of 1.47–1.52 Å accepted for normal $C(sp^2)$–$C(sp^2)$ bonds.[38] This result, being a common feature of planar dithiooxamide derivatives, can be explained by a further consideration of the molecular orbitals of these molecules (vide infra).

The mean value of 1.47 (2) Å for the N–$C(sp^3)$ bonds in **1** is in accordance with the generally accepted values for such bonds (1.47 Å). However, the bond length of 1.477 (7) for C(3)–C(4) is considerably smaller than the value of 1.54 Å for a normal $C(sp^3)$–$C(sp^3)$ bond. We believe that this result arises from a steric effect imposed by the sp^2 configuration of the nitrogen atoms rather than from a partial delocalization of charge along this bond in the six-membered cyclic ligand, since a Newman projection along C(4)–C(3) shows that the N(1)–C(4)–C(3)–N(2) torsion angle in **1** is no less than 57°.

2. $Re(CO)_3$(Cycl-DTO)Br (2). Figure 3 shows the structure of the complex $Re(CO)_3$(Cycl-DTO)Br (**2**). In this complex the cyclic dithiooxamide ligand is also bonded to the metal as a chelate (σ,σ-S,S′; 4e), and it represents the first structurally characterized metal carbonyl complex with a neutral dithiooxamide ligand. The stereochemistry of **2** is facial, which is a common structural feature of $M(CO)_3LX$ (M = Mn, Re; L = bidentate donor; X = halide) complexes.[39-41]

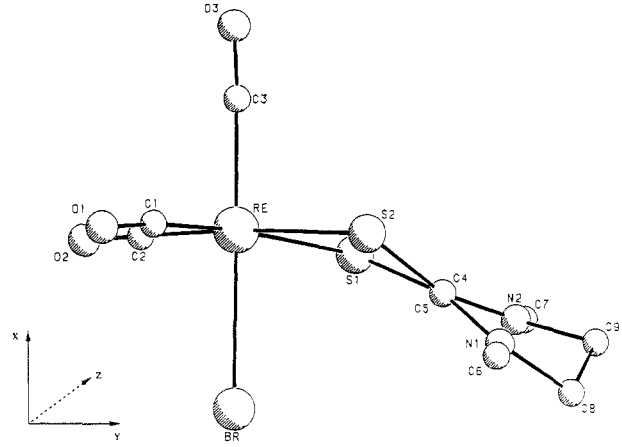

Figure 3. Crystal structure of $Re(CO)_3$(Cycl-DTO)Br (**2**).

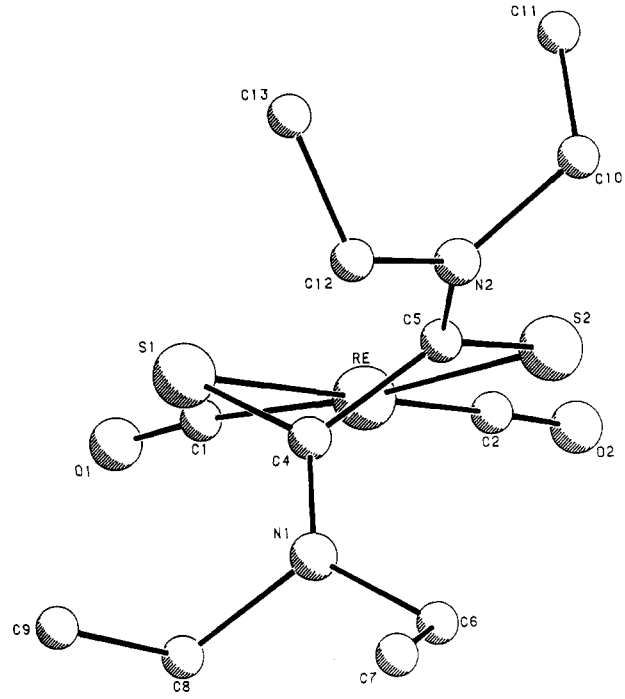

Figure 4. Crystal structure of $Re(CO)_3(Et_4$-DTO)Br (**3**). The axial CO and Br^- ligands have been omitted (see text).

The standard deviation of the calculated equatorial plane through the atoms Re, S(1), S(2), C(1), and C(2) is only 0.04 Å. Figure 3 clearly shows, however, that the DTO ligand itself is bent toward the Re–Br bond. The interplanar angle between the equatorial plane and the calculated plane defined by the DTO S(1), S(2), C(4), C(5), N(1), and N(2) atoms is calculated to be no less than 27.2°. The origin of this behavior will be explained after a further discussion of the electronic properties or this complex (vide infra).

The mean Re–S bond length in **2** is 2.461 (6) Å, which is smaller than the values reported for the complex $Re(CO)_3$(2-methyl-2-(triphenylphosphonio)dithiopropionate)Br (2.488 (1) and 2.503 (1) Å, respectively).[39] The Re–Br distance of 2.643 (1) Å as well as the mean Re–C distance of 1.92 (2) Å equals those observed in other *fac*-$Re(CO)_3LBr$ (L = bidentate donor) complexes.[39-41]

With regard to the geometry within the S,S′-chelated cyclic DTO ligand in **2**, it should be emphasized that with respect to the structure of **1** some interesting changes within the ligand geometry are observed. In the first place the central C–C bond is significantly shorter in **2** than in **1** (1.48 (1) Å compared to

(34) Christensen, A.; Geise, H. J.; Van Der Veken, B. J. *Bull. Soc. Chim. Belg.* **1975**, *84*, 1173.
(35) Adiwidjaja, G.; Voss, J. *Chem. Ber.* **1977**, *110*, 1159.
(36) Hendriksen, L.; Isaksson, R.; Liljefors, T.; Sandström, J. *Acta Chem. Scand.* **1981**, *B35*, 489.
(37) The esd's of the mean values are calculated by $(\sum_i(x_i - x_{mean})/(N-1))^{1/2}$.
(38) Brown, M. G. *Trans. Faraday Soc.* **1959**, *55*, 694.
(39) Winter, W.; Merkel, R.; Kuze, U. *Z. Naturforsch.* **1983**, *38B*, 747.
(40) Couldwell, M. C.; Simpson, J. *J. Chem. Soc., Dalton Trans.* **1979**, 1101.
(41) Abel, E. W.; Bhatti, M. M.; Hursthouse, M. B.; Malik, K. M. A.; Mazid, M. A. *J. Organomet. Chem.* **1980**, 345.

Table VII. Vertical Ionization Potentials and Their Assignments for Several Dithiooxamide Ligands and tBu-DAB

ligand	obsd IP's/eV			
Me_2-DTO[a]	8.23 (n_+)	8.59 (π_-)	9.03 (n_-)	9.03 (π_+)
H_2-DTO[b]	7.90 (n_+)	8.58 (π_-)	8.76 (n_-)	8.81 (π_+)
Cycl-DTO[a]	7.82 (π_-)	7.9 (n_-)	8.1 (n_+)	8.66 (π_+)
tBu-DAB[c]	9.26 (n_-, n_+)	9.78 (π_-)		

[a] Values from ref 37. [b] Calculated, this work. [c] Values from ref 43.

1.532 (5) Å), whereas the mean C–S and C–N bond lengths of the planar thioamide moieties in **2** (1.686 (13) and 1.305 (7) Å, respectively) differ only slightly from those in **1**.

Second, the calculated dihedral angle of 18° between the two planes comprising the thioamide groups in **2** is substantially smaller than the corresponding angle in **1** (θ = 35.4°) and in the complexes $[Cu(Bzl_2\text{-DTO})_2][ClO_4]_2$ (θ = 36.3°) and $Zn(Me_2\text{-DTO})Cl_2$ (θ = 36.9°).[21] In these latter complexes, the torsion around the central C–C bond was explained by a steric strain imposed by the thioamide protons requiring a suitable nonbonded H---H distance. When such a strain was not present, as in the case of Pd-(cHex$_2$-dithiooxamidato)$_2$, a near coplanarity of the two thioamide groups was observed (θ = 0.8°).[21]

3. Re(CO)$_3$(Et$_4$-DTO)Br (3). Figure 4 shows the relevant part of the structure of **3**, visualized in the direction of the dithiooxamide–rhenium bond. In this figure the axial CO and Br$^-$ ligands have been omitted, since their position could not be determined reliably due to the disorder along the CO–Re–Br axis (see Experimental Section). This disordering produces composite electron distributions at the sites of CO and Br, which have to be separated into contributions of C, O, and Br. This separation cannot be very accurate, and especially the parameters of the lighter C and O will be affected. Not much value should therefore be attached to the results for the disordered CO group (both bond distance and bond angle, Table VI) of both isomers.

Figure 4 clearly demonstrates the torsion around the central C–C bond in this complex, and the calculated dihedral angle of 76.9° between the two thioamide groups shows that contrary to that in complex **2**, the Re–SCCS fragment is not planar. Also, the central C(4)–C(5) bond length (1.54 (3) Å) is considerably larger than that for **2** (1.48 (1) Å).

It will be shown hereafter that these structural differences are common for R_4-DTO complexes when compared to those of R_2-DTO and Cycl-DTO.

Theoretical Analysis. LCAO–Xα MO calculations were performed on both the H_2-DTO ligand and the model compound Re(CO)$_3$(H_2-DTO)Br (for details, see Experimental Section). In this complex the H_2-DTO ligand was positioned as a planar molecular in the equatorial plane.

1. H_2-DTO. The molecular orbital orderings for the valence region of both *s-trans*-H_2-DTO and *s-cis*-H_2-DTO agree well with Fenske–Hall molecular orbital calculations on these molecules, reported recently.[15] The geometrical change from s-trans to s-cis only causes minor changes in the electronic structures of these molecules. Regarding the imaginary *s-cis*-H_2-DTO molecule, our results show that the LUMO of this molecule is a low-energy π^* orbital of b_2 symmetry built up mainly by S (49%), C (31%), and N (15%) p_π orbitals. The character of this LUMO with respect to its SCCS part equals that of the corresponding LUMO π^* of an *s-cis*-R-DAB fragment[42] (also with b_2 symmetry), i.e. S–C antibonding and C–C bonding. For *s-cis*-H_2-DTO this orbital is also C-N antibonding in character. The $6b_1$ HOMO of *s-cis*-H_2-DTO has almost entirely sulfur 3p lone-pair (n_-) character. Figure 5A shows an orbital contour plot of this orbital in the plane of the molecule, and it demonstrates that electronic repulsion exists between the two diffuse sulfur 3p orbitals. As a result, a destabilization of this orbital takes place with respect to its $6b_u$ *s-trans*-H_2-DTO analogue, as can be seen by their HFS one-electron energies ($6b_1$ is 1.64 eV higher than $6b_u$). Figure 5A also shows the second sulfur lone-pair (n_+) $7a_1$ orbital of *s-cis*-H_2-DTO, which is stabilized with respect to its $7a_g$ *s-trans*-H_2-DTO analogue because of a mutual overlap between the sulfur 3p orbitals. The orbital contour plots reveal that both the $6b_1$ and the $7a_1$ orbitals of *s-cis*-H_2-DTO have the right symmetry to act as good σ-donor orbitals to a transition-metal center.

The IP's calculated for *s-trans*-H_2-DTO agree well with the experimental values and are shown in Table VII.[41] Since these IP's are all lower in energy than those of tBu-DAB and other α-diimines, the DTO molecules will act as better donor ligands when they are bonded to a metal center as a neutral ligand. In fact our calculations on Re(CO)$_3$(H_2-DTO)Br support this conclusion.

2. Re(CO)$_3$(H_2-DTO)Br. Figure 6 shows the relevant part of the MO diagram of Re(CO)$_3$(H_2-DTO)Br composed from the level ordering diagrams of *s-cis*-H_2-DTO and Re(CO)$_3$Br. First we will briefly describe the electronic structure of the Re(CO)$_3$Br fragment, having C_s symmetry.

At first sight the most striking feature in Figure 6 is the presence of two almost degenerate HOMO's (14a′ and 8a″, respectively) in this fragment, both having predominantly (75%) halogen 4p lone-pair character. However, this ordering is known for M(CO)$_5$X (M = Mn, Re; X = halide) complexes, showing HOMO's that have either metal d (X = Cl) or halogen p (X = I) character.[43]

A manifold of four orbitals is situated at ca. 1.5 eV below these "Br 4p" orbitals, viz. 11a′, 12a′, 13a′, and 7a″. From these the 13a′ orbital has mainly (69%) Br $4p_x$ character but a significant σ-bonding admixture is present in a Re 5d hybrid (with $5d_{xy}$ and $5d_{x^2-y^2}$ character), as shown in the contour plot of this orbital in Figure 5B. This figure also shows the spatial extent of this orbital at the side of the incoming *s-cis*-H_2-DTO molecule, which makes it suitable for overlap with the DTO π system. As the Re(CO)$_3$(H_2-DTO)Br complex has no axial symmetry, the Re–Br σ bond is constructed from orbitals with strongly mixed σ and π overlaps. Thus, apart from the above 13a′ orbital, also 11a′ and 12a′, which are predominantly Re $5d_{z^2}$ and Re $5d_{xy}$ in character, contribute to the bonding to the Br atom and to the three carbonyl groups. From the symmetry of these occupied orbitals a considerable overlap repulsion with occupied orbitals of *s-cis*-H_2-DTO is, however, expected. Finally, the 7a″ orbital is mainly Re $5d_{xz}$ in character.

The two lowest empty orbitals 9a″ and 15a′ of the Re(CO)$_3$Br fragment are both mainly localized on Re, and their orbital contour plots, also shown in Figure 5B, reveal that they are perfectly suited for interaction with the σ-donor orbitals of the *s-cis*-H_2-DTO ligand from Figure 5A.

In the MO diagram of Re(CO)$_3$(H_2-DTO)Br, the LUMO 24a′ has mainly DTO π^* character, the DTO $3b_2$ orbital participating for no less than 87% in this orbital. However, instead of the occupied Re 5d orbitals 11a′ and 12a′, the Br $4p_x$ orbital (13a′) has the largest admixture in this LUMO of the complex. This is not surprising considering the already mentioned possibility of the 13a′ orbital to interact with the DTO π system. The consequences of this interaction will be further discussed hereafter.

The almost degenerate HOMO's 23a′ and 16a″, situated at only 0.35 eV below the LUMO, almost entirely (93%) consist of the Re(CO)$_3$Br fragment 14a′ and 8a″ orbitals and have predominantly Br $4p_y$ and Br $4p_z$ character. At ca. 4.4 eV below these HOMO's, a manifold of five orbitals is observed in Figure 6. From these orbitals the 21a′ and 20a′ have hardly changed their Re 5d character compared to their Re(CO)$_3$Br fragment analogues 11a′ and 12a′. The third filled Re 5d orbital (7a″ Re $5d_{xz}$ in the Re(CO)$_3$Br fragment) mixes in a 1:1 ratio with the DTO $2a_2$ (π_-) orbital giving rise to the 15a″ (antibonding) and 13a″ (bonding) orbitals. The strong interaction between the participating orbitals is antibonding, since these orbitals are both occupied. The complex 22a′ orbital is built up mainly (71%) by the 13a′ orbital (with Br $4p_x$ character) of the Re(CO)$_3$Br fragment, albeit with a significant contribution from the DTO $2b_2$ and $3b_2$ orbitals (together 26%). This again reflects the

(42) Louwen, J. N.; Stufkens, D. J.; Oskam, A. *J. Chem. Soc., Dalton Trans.* **1984**, 2683.

(43) Jolly, W. L. *J. Phys. Chem.* **1983**, *87*, 26.

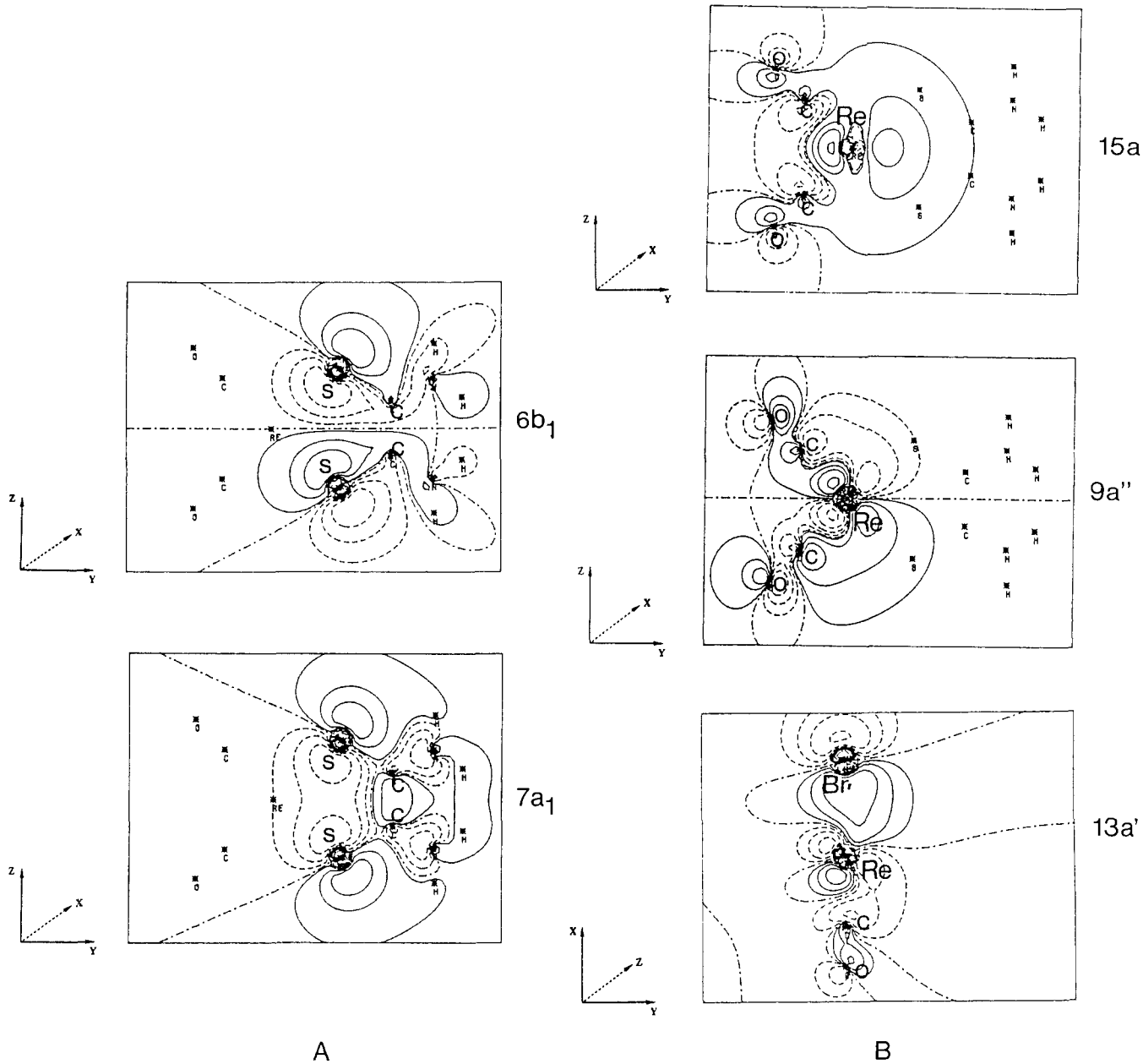

Figure 5. (A) Orbital contour plots of the *s-cis*-H_2-DTO fragment highest occupied sulfur lone-pair orbitals in the *yz* plane $6b_1$ (n_-, HOMO) and $7a_1$ (n_+). (B) Orbital contour plots of the $Re(CO)_3Br$ fragment 15a' (*yz* plane), 9a'' (LUMO; *yz* plane) and 13a' (*xy* plane) orbitals.

suitability of the 13a' fragment orbital to overlap with the ligand π system. Finally, an important σ-bonding interaction between the DTO ligand and the metal fragment gives rise to the complex 14a'' level. The largest contributions to this level arise from the *s-cis*-H_2-DTO HOMO $6b_1$ (n_-; see Figure 5A) and the $Re(CO)_3Br$ LUMO 9a'' (Re $5d_{yz}$; see Figure 5B) orbitals. The antibonding combination of these orbitals, 17a'', is situated no less than 2.5 eV above the complex LUMO 24a'.

At ca. 0.8 eV below the complex 14a'' level the MO scheme shows two orbitals that are both important with respect to the bonding and electronic transitions of the complex. Apart from the above-mentioned 13a'' orbital, the 19a' orbital has contributions from the occupied DTO $7a_1(n_+)$ and the empty $Re(CO)_3Br$ 15a' (Re *dsp*) orbitals, giving rise to a DTO to metal σ donation.

Electronic Absorption Spectra. The relevant electronic absorption spectral data for **1** and for the complexes under study are collected in Table VIII. The absorption spectra of complexes **2**–**4** are depicted in Figure 7.

The spectra of the complexes **2** and **4** show two intense absorption bands ($\epsilon \cong 4 \times 10^3$ M^{-1} cm^{-1}), the lowest energy one being situated at ca. 530 nm for both complexes. The position, intensity, and in particular the large solvatochromism of the latter band (derived from the spectra taken in chloroform and acetonitrile) all point to a transition with considerable Re to DTO charge-transfer character.

The high-energy absorption bands of **2** and **4** also exhibit a significant solvatochromism, and they must therefore also belong to transitions having MLCT character. However, in this spectral region LF transitions are also expected to occur. With respect

Table VIII. Electronic Absorption Spectral Data[a]

compd	λ^{max}/ nm	ϵ^{max}/ M^{-1} cm^{-1}	Δ^{max}/ 10^3 cm^{-1} [b]
Cycl-DTO (**1**)	410 sh	(500)[c]	
	314	11000	0.3
$Re(CO)_3$(Cycl-DTO)Br (**2**)	542	4500	2.0
	373	4600	1.3
$Re(CO)_3$(Et_4-DTO)Br (**3**)	434 sh	(2100)[c]	
	322 sh	(5400)[c]	
$Re(CO)_3$(Bzl_2-DTO)Br (**4**)	524	3800	1.4
	356	4100	1.0
$Re(CO)_3$(Cycl-DTO)Cl (**5**)[d]	522		
	338		

[a] Measured in chloroform. [b] $\Delta^{max} = \sigma^{max}(CH_3CN) - \sigma^{max}(CHCl_3)$. [c] ϵ^{max} of strongly overlapping bands. [d] Measured in situ in acetone (see text).

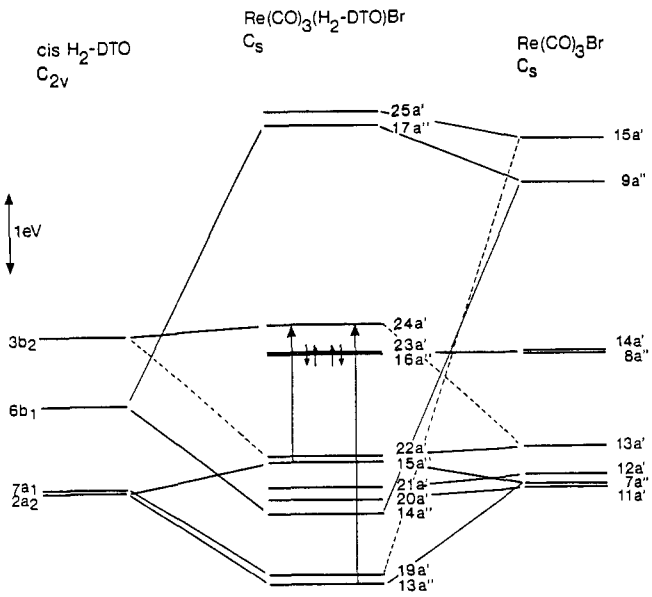

Figure 6. Relevant part of the MO diagram of Re(CO)$_3$(H$_2$-DTO)Br.

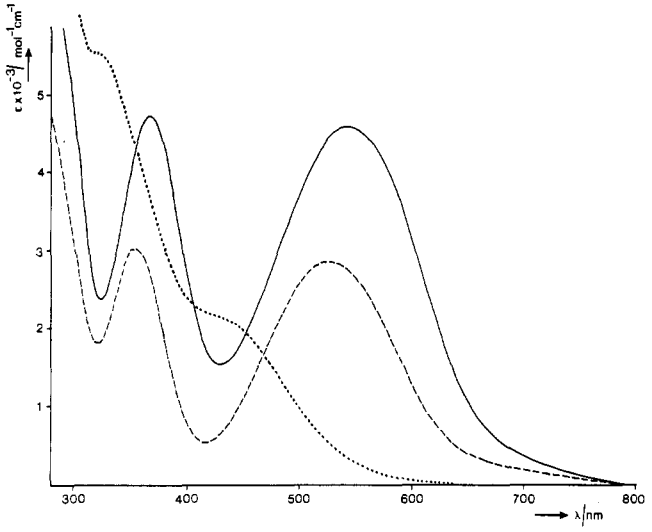

Figure 7. Electronic absorption spectra at 293 K in chloroform of Re(CO)$_3$(Cycl-DTO)Br (—), Re(CO)$_3$(Bzl$_2$-DTO)Br (- - -), and Re(CO)$_3$(Et$_4$-DTO)Br (···).

to these LF transitions it should be emphasized that for Re(CO)$_5$Br the LF $^1E \leftarrow {}^1A_1$ transition is found at 326 nm in EPA[44] whereas for Re(CO)$_3$(α-diimine)Br[8,45] and Re(CO)$_3$(py)$_2$Br[46] these weak LF transitions were proposed to be obscured by the more intense MLCT or IL transitions. Thus, the 360-nm band of complexes **2** and **4** may also contain a LF transition and this suggestion is confirmed by the photochemistry of these complexes.[22]

Contrary to those of the complexes **2** and **4**, the spectrum of **3** does not show a low-energy MLCT band but instead a lowest energy shoulder at ca. 434 nm (Figure 7). Similar differences between the UV/vis spectra of R$_2$-DTO and R$_4$-DTO complexes have been reported by tom Dieck et al.[20] These results can be attributed to the structural differences between the DTO ligands in these complexes (vide infra).

Resonance Raman Spectra. RR effects are expected to occur for complexes with MLCT transitions provided that no close-lying LF transitions are present, which will give rise to a deenhancement of the Raman intensities.[47] Thus, rR spectra could only be obtained for the complexes **2** and **4**, which have isolated MLCT bands in their absorption spectra. Relatively weak rR effects were observed by excitation into these MLCT transitions. Furthermore, excitation at different wavelengths within the MLCT band hardly changed the RR spectra of these complexes. Resonance enhancement of Raman intensity was only observed for several ligand modes and for one carbonyl stretching mode. Hardly any rR effect could be observed for the low-energy vibrations. The rR spectrum of **2**, taken in CH_2Cl_2, is shown in Figure 8.

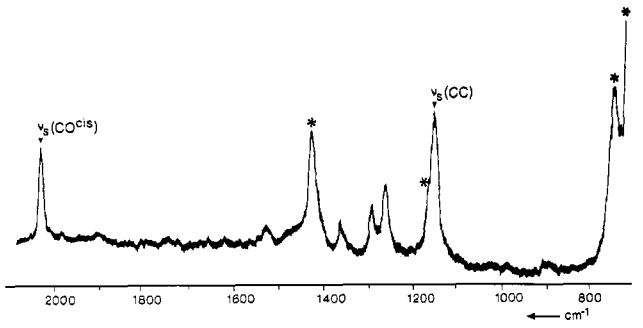

Figure 8. Resonance Raman spectrum of Re(CO)$_3$(Cycl-DTO)Br (**2**) upon excitation with the 488-nm laser line. The bands indicated with an asterisk belong to the solvent CH_2Cl_2.

Table IX. One-Electron Energies of Free Re(CO)$_3$Br and *cis*-H$_2$-DTO Fragment Orbitals and Gross Orbital Populations in Re(CO)$_3$(H$_2$-DTO)Br

orbital	type	orbital energy/eV	pop. of electrons
	Re(CO)$_3$Br		
11a'	Re 5d$_{z^2}$ + 5d$_{xy}$	−7.56	1.957
12a'	Re 5d$_{xy}$ + 5d$_{z^2}$	−7.43	1.976
13a'	Br 4p$_x$	−7.10	1.870
14a'	Br 4p$_y$	−5.89	1.953
15a'	Re dsp	−3.19	0.215
16a'	CO$_{eq}$ π^*	−2.04	0.030
17a'−50a'			0.076
7a''	Re 5d$_{xz}$	−7.54	1.996
8a''	Br 4p$_z$	−5.96	1.982
9a''	Re 5d$_{yz}$	−3.78	0.324
10a''−31a''			0.064
	cis-H$_2$-DTO		
7a$_1$	S lp (n$_+$)	−5.14	1.738
2a$_2$	π	−5.14	1.982
6b$_1$	S lp (n$_-$)	−4.02	1.687
2b$_2$	π	−6.05	1.968
3b$_2$	π^*	−3.08	0.212

The strongest rR effect is observed for a Raman band a 1149 cm^{-1}. According to the literature[48,49] this band will have predominantly ν_s(CC) character, ν_s(CC) being the symmetric stretching vibration of the central carbon atoms of the DTO ligand. This rR effect is not remarkable, since the π^* orbital of Cycl-DTO is π bonding along the C–C bond (vide supra). The MLCT transition to this π^* orbital will therefore be accompanied by a shortening of the C–C bond and accordingly by a rR effect for ν_s(CC). The absence of a strong rR effect for the ν_s(CS) and ν_s(CN) modes (observed at 832 and 1440 cm^{-1}, respectively, in the Raman spectrum of H$_2$-DTO[48]) indicates that these bonds are much less affected by this transition. Apparently, the effects of population of the π^* orbital, being both CS and CN antibonding, are compensated by a different electronic interaction with the metal center.

Finally, the appearance of a rR effect for $\nu_s(CO^{cis})$ is in accordance with rR results published by us for Re(CO)$_3$LX (L = α-diimine; X = halide) and M(CO)$_4$L (L = α-diimine) com-

(44) Wrighton, M. S.; Morse, D. L.; Gray, H. B.; Ottesen, D. K. *J. Am. Chem. Soc.* **1976**, *98*, 1111.
(45) Wrighton, M. S.; Morse, D. L. *J. Am. Chem. Soc.* **1974**, *96*, 998.
(46) Wrighton, M. S.; Morse, D. L.; Pdungsap, L. *J. Am. Chem. Soc.* **1975**, *97*, 2073.
(47) Stein, P.; Miskowski, V.; Woodruff, W. H.; Griffin, J. P.; Werner, K. G.; Gaber, B. P.; Spiro, T. G. *J. Chem. Phys.* **1976**, *64*, 2159.
(48) Desseyn, H. O.; Van Der Veken, B. J.; Aarts, A. *Can. J. Spectrosc.* **1977**, *22*, 84.
(49) Stufkens, D. J.; Snoeck, Th. L.; Van Der Veken, B. J. *Inorg. Chim. Acta* **1983**, *76*, L253.

Table X. Overlaps of Selected $Re(CO)_3Br$ Orbitals with Frontier Orbitals of *cis*-H_2-DTO

	cis-H_2-DTO				
$Re(CO)_3Br$	$7a_1$ (S lp)	$6b_1$ (S lp)	$2a_2$ (π)	$2b_2$ (π)	$3b_2$ (π^*)
11a′ (Re 5d)	−0.041	0	0	0.063	0.045
12a′ (Re 5d)	0.033	0	0	0.044	0.028
13a′ (Br $4p_x$)	−0.021	0	0	0.108	0.098
14a′ (Br $4p_y$)	−0.107	0	0	0.005	0.001
15a′ (Re dsp)	−0.272	0	0	−0.050	−0.041
7a″ (Re $5d_{xz}$)	0	−0.090	0.121	0	0
8a″ (Br $4p_z$)	0	−0.085	0.004	0	0
9a″ (Re $5d_{yz}$)	0	0.222	0.010	0	0

plexes.[7,8] This effect is explained by a partial delocalization of the MLCT excited states over the carbonyl groups.

Discussion

Electronic Interactions. For a better understanding of the various electronic interactions in $Re(CO)_3(H_2$-DTO)Br, the results of the SCF calculations were further examined. Table IX shows some Mulliken gross orbital populations of relevant fragment valence orbitals in the $Re(CO)_3(H_2$-DTO)Br complex as well as orbital energies of the fragment orbitals. Furthermore, Table X presents some relevant overlap data, which are a measure for the strengths of the interactions observed.

It is clear from Table IX that the three orbitals representing the filled Re 5d orbitals, i.e. 11a′, 12a′, and 7a″, hardly show any decrease in population upon interaction with *cis*-H_2-DTO. This implies that metal to DTO back-bonding does not take place from these orbitals. It is obvious from Table X that the lack of overlap between these orbitals and the DTO π^* orbital is responsible for this effect. On the other hand, a significant reduction in population of the 13a′ orbital (0.13 e) having substantial Br $4p_x$ character is observed in Table IX due to a considerable overlap of this orbital with the DTO π^* orbital (see Table X). Thus, $Re(CO)_3Br$ to π^* DTO back-donation occurs essentially from an orbital with substantial Br 4p character (69%) and with only little Re d_{xy} character (8%). This result, which had already been expected from the orbital contour plot of the 13a′ orbital in Figure 5B, is further established by the remarkable bending of the DTO ligand in the direction of the Re–Br bond shown in the crystal structure of **2** (Figure 3).

Table IX shows that the $Re(CO)_3Br$ 15a′ (Re dsp hybrid) and 9a″ (Re $5d_{yz}$) orbitals both serve as σ acceptors and relatively much charge (0.22 and 0.32 e, respectively) is donated into these orbitals. Table X nicely shows that this interaction originates from the strong overlap of 15a′ with the DTO $7a_1(n_+)$ orbital (0.27) and of 9a″ with the DTO $6b_1$ (n_-) orbital (0.22). The electronic charge in the other high-lying virtuals of $Re(CO)_3Br$ reflects small charge transfers from *s-cis*-H_2-DTO and also polarization of $Re(CO)_3Br$ itself.

The observed population changes of the relevant orbitals of *s-cis*-H_2-DTO confirm the conclusions about the bonding toward the $Re(CO)_3Br$ fragment discussed above. In addition it can be said that both sulfur lone-pair $6b_1$ and $7a_1$ orbitals serve as good σ-donor orbitals. Together they donate 0.58 e to the metal fragment. On the other hand, the inertness of the populations of the π orbitals $2a_2$ and $2b_2$ of the DTO ligand suggests that this ligand will not act as a good π-donor ligand.

The interaction between the DTO π^* $3b_2$ orbital and the $Re(CO)_3Br$ fragment results in a donation of 0.21 e to this DTO π^* orbital, which is therefore a good π-accepting orbital. This significant charge donation into the DTO π^* orbital will cause a strengthening of the central C–C bond of the DTO ligand, since the π^* orbital is strongly π bonding along this bond. As a consequence, the C–C bond of **2** (1.48 (1) Å) is significantly shorter than that of the free ligand **1** (1.532 (5) Å).

Electronic Transitions. 1. DTO Ligands. From the π orbitals of *s-trans*-H_2-DTO having b_g and a_u symmetry, respectively, only $2b_g$ gives rise to a symmetry-allowed $\pi \rightarrow \pi^*$ ($2b_g \rightarrow 3a_u$) transition.[15] This transition is the most intense one in the absorption spectra of *s-trans*-R_2-DTO ligands and is normally observed at ca. 310 nm.[36,50-53] The weak broad band in the visible region, exhibiting vibrational fine structure at lower temperatures,[15] has been assigned to an $n \rightarrow \pi^*$ ($7a_g \rightarrow 3a_u$) transition.

For *s-cis*-R_2-DTO ligands, $\pi \rightarrow \pi^*$ transitions are allowed from both π orbitals in the valence region (having a_2 and b_2 symmetry, respectively). One of these transitions, $2b_2 \rightarrow 3b_2$, will, however, be higher in energy by ca. 0.9 eV than the other one ($2a_2 \rightarrow 3b_2$; see Table IX). The spectra of *s-cis*-R_2-DTO ligands in the near UV/visible region are therefore quite similar to those of their s-trans analogues. They show a strong $\pi \rightarrow \pi^*$ ($2a_2 \rightarrow 3b_2$) transition and a weak $n \rightarrow \pi^*$ ($7a_1 \rightarrow 3b_2$) one at lower energy. The spectral data for **1** (Table VIII) confirm this agreement.

2. $Re(CO)_3$(DTO)Br Complexes. As a rule, when the direction of charge transfer during a transition is parallel to the induced electric dipole, that particular transition is expected to be the most intense in the absorption spectrum.[54] For this reason transitions of $Re(CO)_3(H_2$-DTO)Br polarized along the y axis will be the strongest ones. As a consequence, only transitions of the type a″ → a′ are expected to be intense, since these are all x,y polarized whereas the a′ → a′ transitions are all z polarized and therefore expected to be weak. With this restriction only four transitions from the nine symmetry-allowed ones in the MO diagram of Figure 6 have to be taken into account, viz. a Br(4p) → L(π^*) transition (16a″ → 24a′), a Re($5d_{xz}$)–L(π) → L(π^*) transition (15a″ → 24a′), a ligand-based $n \rightarrow \pi^*$ transition (14a″ → 24a′), and a Re($5d_{xz}$) + L(π) → L(π^*) transition (13a″ → 24a′). From these transitions the 16a″ → 24a′ (Br($4p_z$) → L(π^*)) one is expected to be very weak due to mutual orthogonality of the 16a″ and 24a′ orbitals. The same holds for the 14a″ → 24a′ ($n \rightarrow \pi^*$) transition, which is also rather weak in the absorption spectra of free DTO ligands.[50-53] As a consequence, only two transitions, viz. 15a″ → 24a′ (Re($5d_{xz}$)–L(π) → L(π^*)) and 13a″ → 24a′ (Re($5d_{xz}$) + L(π) → L(π^*)), will be intense, and they are expected to dominate the electronic absorption spectrum. These transitions, depicted by arrows in the MO scheme of Figure 6, will both possess Re to DTO charge-transfer character. For $Re(CO)_3(H_2$-DTO)Br a value of 1.53 eV has been calculated for the energy difference between these two transitions. They are therefore expected to occur separately in the electronic absorption spectrum. Indeed the spectra of the complexes **2** and **4** (Figure 7) confirm the above qualitative picture, in spite of the fact that $\theta > 0°$ will prohibit a pure C_s symmetry (as in the calculations) for these complexes.

Because a qualitative correlation exists between the calculations for $Re(CO)_3(H_2$-DTO)Br and the experimental data for **2** or **4**, we can take into account the influence of this dihedral angle θ between the two thioamide groups on the electronic absorption spectra. This angle was 0° in the calculations on $Re(CO)_3(H_2$-DTO)Br and 18° from the crystal structure of **2**, and it is expected to be >30° for **4** due to steric strain caused by the thioamide protons.[21] For this purpose a correlation diagram has been constructed for the energies of the ligand valence orbitals in relation to this dihedral angle. This diagram is shown in Figure 9 for dihedral angles between 0 and 90°.

Regarding this figure, it should be emphasized that the symmetry of the H_2-DTO ligand with $0° < \theta \leq 90°$ is always C_2. Furthermore, there are no avoided crossing effects due to the intersection of orbitals with the same symmetry (being a or b), although the calculations show that for ⊥-H_2-DTO ($\theta = 90°$) some interaction exists between the 7b (π) and 8b (n) orbitals. As θ increases, the LUMO π^* will destabilize until for $\theta = 90°$ two completely degenerate π^* LUMO's are present. The HOMO n_+ will stabilize with increasing values for θ due to a decrease of electronic overlap repulsion between the sulfur lone-pair orbitals (see also Figure 5). For similar reasons the n_- orbital will destabilize.

Importantly, the stabilization of the $2a_2$ π orbital upon increasing the dihedral angle will directly affect the character of

(50) Persson, B.; Sandström, J. *Acta Chem. Scand.* **1964**, *18*, 1059.
(51) Larson, D. B.; McGlynn, S. P. *J. Mol. Spectrosc.* **1973**, *47*, 469.
(52) Isaksson, R.; Liljefors, T. *J. Chem. Soc., Perkin Trans. 2* **1980**, 1815.
(53) Isaksson, R.; Liljefors, T. *J. Chem. Soc., Perkin Trans. 2* **1981**, 1344.
(54) Day, P.; Sanders, N. *J. Chem. Soc. A* **1967**, 1536.

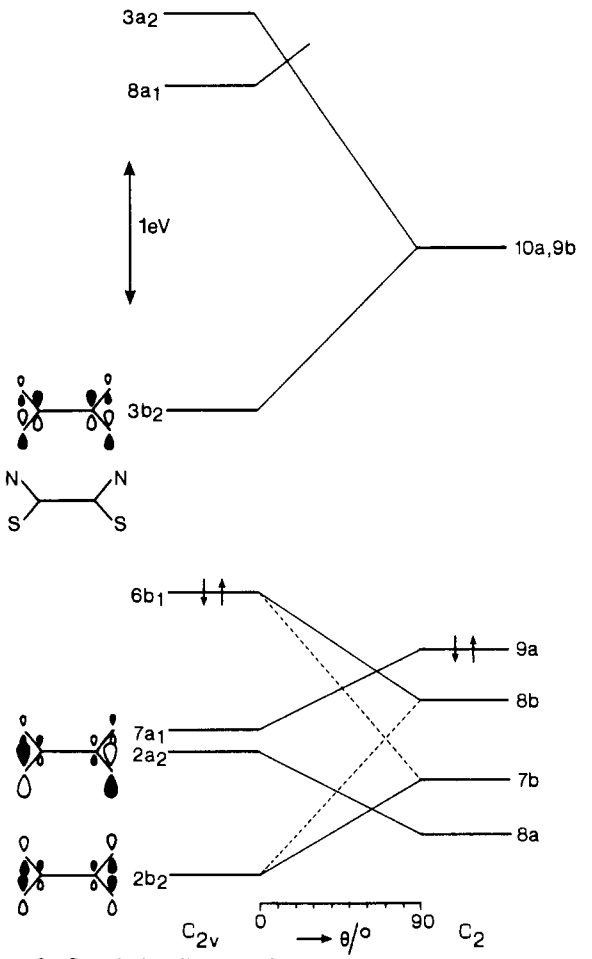

Figure 9. Correlation diagram of the valence orbitals of *s-cis*-H_2-DTO upon varying the dihedral angle θ from 0 to 90°. The symmetry of the molecule thereby changes from C_{2v} (θ = 0°) to C_2 (0° < $\theta \leq$ 90°).

the MLCT transitions of the corresponding $Re(CO)_3LBr$ complexes (vide supra), provided that the orbitals of the $Re(CO)_3Br$ fragment in all complexes are at the same energies as for $Re(CO)_3(H_2$-DTO)Br. This stabilization will decrease the mixing with the Re $5d_{xz}$ orbital and as a result the lowest energy $Re(5d_{xz})$–$L(\pi) \rightarrow L(\pi^*)$ transition will have the strongest MLCT character. This prediction is nicely confirmed by the absorption data for **2** and **4** (Table VIII). For both complexes a stronger solvatochromism of the low-energy MLCT transition is found.

The occurrence of electronic transitions in the 300–600-nm region originating from the two complex HOMO's with Br 4p character can be excluded not only on the basis of arguments given above but also by comparison of the spectra of the complexes **2** and $Re(CO)_3$(Cycl-DTO)Cl (**5**). These spectra are completely similar. Apparently, stabilization of the Cl 3p with respect to the Br 4p orbitals hardly affects the positions of the MLCT transitions in the spectra of these complexes.

So, the experimental as well as the theoretical results lead to a straightforward assignment of the two intense transitions in the absorption spectra of **2**, **4**, and **5** to two transitions with predominantly Re(5d) → DTO(π^*) charge-transfer character. In contrast with this, complex **3** (θ = 79.6°) does not show such low-energy MLCT transitions due to the destabilization of the DTO π^* orbital with increasing dihedral angle (compare Figures 7 and 9). This destabilization is caused by the lack of overlap between the two π^* orbitals of the thioamide groups at sufficient large dihedral angles.

Structural Differences. The preceding sections demonstrate that the theoretical data of H_2-DTO and its $Re(CO)_3(H_2$-DTO)Br complex can be used to describe the character of the lowest energy transitions of the complexes under study and to predict their mutual positions. These theoretical results can, however, also be used to explain the structural differences among **1**–**3**. The differences between **1** and **2** concern first of all the dihedral angle between the thioamide groups, which decreases from 35.4 to 18° upon complexation of **1**. This effect is mainly due to the decrease of repulsion between the sulfur p orbitals. In the free ligand this repulsion is rather strong, giving rise to the dihedral angle of 35.4°. In complex **2** the repulsion is reduced by the σ-bonding interaction of these sulfur p orbitals in the equatorial plane (see Figure 5A) with orbitals mainly localized on Re.

With respect to the shortening of the central C–C bond upon going from **1** to **2**, it is of importance to note that planarity will not cause a shortening of this bond, since the π orbitals of the thioamide groups do not give net bonding (for θ = 0°, see Figure 9). This is evident from the calculations on H_2-DTO both in its s-cis (θ = 0°) and its s-trans (θ = 180°) conformation. It is also not likely that this C–C bond shortening is caused by the above-mentioned decrease of repulsion between the sulfur p orbitals upon complexation. In that case a similar short distance would have been expected for **3**. As mentioned before, the most likely explanation for the relatively short C–C distance in **2** is charge donation from the $Re(CO)_3Br$ fragment 13a′ orbital into the π^* orbital of the DTO ligand. This orbital is bonding along the C–C bond when the dihedral angle is small as in **2**. The significant contribution of the C π orbitals to this complex π^* orbital was nicely demonstrated by the rR spectra of **2** upon MLCT excitation, showing the strongest rR effect for ν_s(CC). For complex **3** the large dihedral angle (θ = 79.6°) is caused by the strong steric interaction between the ethyl groups at the thioamide nitrogen atoms.

Acknowledgment. We wish to thank P. Dettmers for performing the first experiments leading to this study and W. G. J. de Lange for his assistance during the preparations.

Registry No. **1**, 78134-03-9; **2**, 122677-54-7; **3**, 122677-55-8; **4**, 122677-56-9; **5**, 122700-86-1; $Re(CO)_5Br$, 14220-21-4; $Re(CO)_3(H_2$-DTO)Br, 122677-57-0; $Re(CO)_3$(Cycl-DTO)$^+$(OTF)$^-$, 122677-59-2.